

The role of Fenton's reaction in aqueous phase pulsed streamer corona reactors

David R. Grymonpré^a, Amit K. Sharma^b, Wright C. Finney^a, Bruce R. Locke^{a,*}

^a Department of Chemical Engineering, FAMU-FSU College of Engineering, Florida State University and Florida A&M University, 2525 Pottsdamer Street, Tallahassee, FL 32310-6046, USA

^b Rhodia, Inc., 259 Prospect Plains Road, Cranbury, NJ 08512, USA

Received 2 June 2000; accepted 14 November 2000

Abstract

Aqueous phase pulsed streamer corona reactors are currently under development for a number of applications including water and wastewater treatment. Previous research has demonstrated that a high voltage pulsed electrical discharge directly into water leads to the formation of reactive species such as hydrogen peroxide and hydroxyl radicals. Since significant quantities of hydrogen peroxide are produced, the role of Fenton's reactions in the pulsed corona reactor is analyzed both experimentally and with computer simulations in the present work. Experimental data shows the existence of optimal iron concentrations for the degradation of phenol, and that the formation of hydrogen peroxide by the pulsed corona discharge is dependent upon both the applied electric field and the solution conductivity. A mathematical model based upon mass balances for 31 radical and molecular species in the batch reactor (including 71 chemical reactions) has been developed and sensitivity analysis performed to identify key reactions. This model is used to show the effects of initial reaction conditions (including iron and phenol concentrations) on the degradation of phenol and the formation of reaction intermediate products and by-products. The model results are in qualitative and semi-quantitative agreement with the experimental observations on the effects of initial iron and phenol concentrations on phenol degradation and by-product formation. © 2001 Elsevier Science B.V. All rights reserved.

Keywords: Fenton's reaction; Streamer corona reactors; Aqueous phase

1. Introduction

The discharge of high voltage electrical pulses directly into water has been of interest for many years due to its importance in electrical transmission processes [1–3] and for its applications in biology [4–7]. More recently, a pulsed electrical discharge in water has been shown to be effective at degrading a number of small organic compounds including phenols [8–10] and organic dyes [11], and at deactivating viruses, bacteria, and yeast [4,5,11–15].

A high voltage pulsed electrical discharge in water leads to both physical and chemical processes that can directly or indirectly degrade organic compounds (for a more extensive review see [16]). Physical processes include the formation of ultraviolet light [17,18] and shock waves [10,19,20], and the magnitude of the contributions of these factors depends strongly upon the energy of the discharge. Capacitor discharge in the kJ per pulse range leads to very intense shock waves [17,18] and large quantities of UV light [17,19,20],

while capacitor discharge in the J per pulse range may lead to more efficient direct production of reactive chemical species.

Chemical processes that occur in electrical discharges in water include the direct formation of reactive radicals such as hydroxyl, hydrogen, superoxide, perhydroxyl, and oxide anions, and molecular species such as hydrogen peroxide and ozone (with gas bubbling at the high voltage electrode). Although many studies have dealt with the physical processes that occur in liquid phase pulsed discharges (e.g. [1,2,21]), a complete understanding of the propagation and formation of streamer discharge in water is not available. In addition, the analysis of the chemical processes that occur in liquid phase pulsed electrical discharge is also incomplete.

Clements et al. [22] demonstrated by emissions spectroscopy that pulsed electrical discharges in water leads to the formation of hydrogen radicals, causes the degradation of dye, and forms ozone upon the bubbling of oxygen through the high voltage electrode. Sharma et al. [8] demonstrated that phenol could be degraded in liquid phase pulsed corona reactors, and that the degradation was strongly dependent upon the presence of iron salts. It was inferred that the increased removal of phenol in the presence of iron (ferrous sulfate) was due to the well known Fenton's reaction [23,24],

* Corresponding author. Tel.: +1-850-410-6165; fax: +1-850-410-6150.
E-mail address: locke@eng.fsu.edu (B.R. Locke).

Table 1
Chemical reactions used in the model

Reaction no.	Reaction
1	$\text{H}_2\text{O} \xrightarrow{k_1} \text{H}^\bullet + \bullet\text{OH}$
2	$\text{H}_2\text{O} \xrightarrow{k_2} \frac{1}{2}\text{H}_2\text{O}_2 + \frac{1}{2}\text{H}_2$
3	$\text{H}_2\text{O} \xrightarrow{k_3} \text{H}^+ + \text{e}_{\text{aq}}^- + \bullet\text{OH}$
4	$\text{Fe}^{3+} + \text{H}_2\text{O}_2 \xrightarrow{k_4} \text{Fe}^{2+} + \text{HO}_2^\bullet + \text{H}^+$
5	$\text{Fe}^{2+} + \text{H}_2\text{O}_2 \xrightarrow{k_5} \text{Fe}^{3+} + \text{OH}^- + \bullet\text{OH}$
6	$\bullet\text{OH} + \text{Fe}^{2+} \xrightarrow{k_6} \text{Fe}^{3+} + \text{OH}^-$
7	$\text{Fe}^{3+} + \text{HO}_2^\bullet \xrightarrow{k_7} \text{Fe}^{2+} + \text{O}_2 + \text{H}^+$
8	$\text{Fe}^{2+} + \text{HO}_2^\bullet \xrightarrow{k_8} \text{Fe}^{3+} + \text{H}_2\text{O}_2$
9	$\text{Fe}^{3+} + \text{O}_2^{\bullet-} \xrightarrow{k_9} \text{Fe}^{2+} + \text{O}_2$
10	$\text{Fe}^{2+} + \text{O}_2^{\bullet-} \xrightarrow{k_{10}} \text{Fe}^{3+} + \text{H}_2\text{O}_2$
11	$\text{e}_{\text{aq}}^- + \text{Fe}^{3+} \xrightarrow{k_{11}} \text{Fe}^{2+}$
12	$\text{H}^\bullet + \text{Fe}^{3+} \xrightarrow{k_{12}} \text{Fe}^{3+} + \text{H}^+$
13	$\bullet\text{OH} + \text{H}_2\text{O}_2 \xrightarrow{k_{13}} \text{HO}_2^\bullet + \text{H}_2\text{O}$
14	$\text{HO}_2^\bullet \xrightarrow{k_{14}} \text{O}_2^{\bullet-} + \text{H}^+$
15	$\text{O}_2^{\bullet-} + \text{H}^+ \xrightarrow{k_{15}} \text{HO}_2^\bullet$
16	$\text{HO}_2^\bullet + \text{HO}_2^\bullet \xrightarrow{k_{16}} \text{H}_2\text{O}_2 + \text{O}_2$
17	$\text{HO}_2^\bullet + \text{O}_2^{\bullet-} \xrightarrow{k_{17}} \text{H}_2\text{O}_2 + \text{O}_2$
18	$\bullet\text{OH} + \text{H}_2 \xrightarrow{k_{18}} \text{H}^\bullet + \text{H}_2\text{O}$
19	$\bullet\text{OH} + \text{O}_2^{\bullet-} \xrightarrow{k_{19}} \text{O}_2 + \text{OH}^-$
20	$\bullet\text{OH} + \text{HO}_2^\bullet \xrightarrow{k_{20}} \text{H}_2\text{O} + \text{O}_2$
21	$2\bullet\text{OH} \xrightarrow{k_{21}} \text{H}_2\text{O}_2$
22	$\bullet\text{OH} + \text{OH}^- \xrightarrow{k_{22}} \text{H}_2\text{O} + \text{O}^{\bullet-}$
23	$\bullet\text{OH} + \text{H}_2\text{O}_2 \xrightarrow{k_{23}} \text{O}_2^{\bullet-} + \text{H}_2\text{O}$
24	$\bullet\text{OH} + \text{O}^{\bullet-} \xrightarrow{k_{24}} \text{HO}_2^-$
25	$\bullet\text{OH} + \text{HO}_2^- \xrightarrow{k_{25}} \text{HO}_2^\bullet + \text{OH}^-$
26	$\text{e}_{\text{aq}}^- + \text{H}^\bullet \xrightarrow{k_{26}} \text{H}_2 + \text{OH}^-$
27	$2\text{e}_{\text{aq}}^- \xrightarrow{k_{27}} 2\text{OH}^- + \text{H}_2$
28	$\text{e}_{\text{aq}}^- + \text{H}_2\text{O}_2 \xrightarrow{k_{28}} \bullet\text{OH} + \text{OH}^-$
29	$\text{e}_{\text{aq}}^- + \text{O}_2 \xrightarrow{k_{29}} \text{O}_2^{\bullet-}$
30	$\text{e}_{\text{aq}}^- + \text{O}_2^{\bullet-} \xrightarrow{k_{30}} \text{O}_2^{2-}$
31	$\text{e}_{\text{aq}}^- + \text{H}^+ \xrightarrow{k_{31}} \text{H}^\bullet$
32	$\text{e}_{\text{aq}}^- \xrightarrow{k_{32}} \text{H}^\bullet + \text{OH}^-$
33	$\text{e}_{\text{aq}}^- + \text{HO}_2^- \xrightarrow{k_{33}} 2\text{OH}^- + \bullet\text{OH}$
34	$\text{e}_{\text{aq}}^- + \bullet\text{OH} \xrightarrow{k_{34}} \text{OH}^-$
35	$\text{e}_{\text{aq}}^- + \text{O}^{\bullet-} \xrightarrow{k_{35}} 2\text{OH}^-$
36	$\text{H}^\bullet + \text{O}_2 \xrightarrow{k_{36}} \text{HO}_2^\bullet$
37	$\text{H}^\bullet + \text{O}_2 \xrightarrow{k_{37}} \text{HO}_2^-$
38	$2\text{H}^\bullet \xrightarrow{k_{38}} \text{H}_2$
39	$\text{H}^\bullet + \bullet\text{OH} \xrightarrow{k_{39}} \text{H}_2\text{O}$
40	$\text{H}^\bullet + \text{HO}_2^\bullet \xrightarrow{k_{40}} \text{H}_2\text{O}_2$
41	$\text{H}^\bullet + \text{H}_2\text{O}_2 \xrightarrow{k_{41}} \text{H}_2\text{O} + \bullet\text{OH}$
42	$\text{H}^\bullet + \text{OH}^- \xrightarrow{k_{42}} \text{e}_{\text{aq}}^- + \text{H}_2\text{O}$
43	$\text{H}^\bullet + \text{H}_2\text{O} \xrightarrow{k_{43}} \text{H}_2 + \bullet\text{OH}$
44	$\text{O}^{\bullet-} + \text{H}_2\text{O} \xrightarrow{k_{44}} \bullet\text{OH} + \text{OH}^-$
45	$\text{O}^{\bullet-} + \text{HO}_2^- \xrightarrow{k_{45}} \text{O}_2^{\bullet-} + \text{OH}^-$
46	$\text{O}^{\bullet-} + \text{H}_2 \xrightarrow{k_{46}} \text{H}^\bullet + \text{OH}^-$
47	$\text{O}^{\bullet-} + \text{H}_2\text{O}_2 \xrightarrow{k_{47}} \text{O}_2^{\bullet-} + \text{H}_2\text{O}$

Table 1 (Continued)

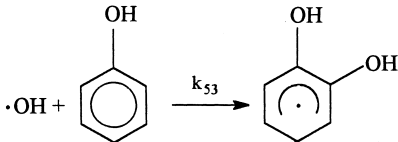
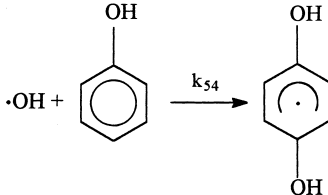
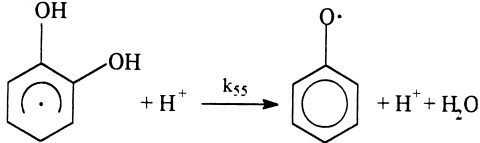
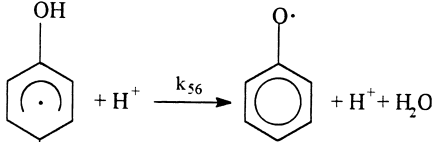
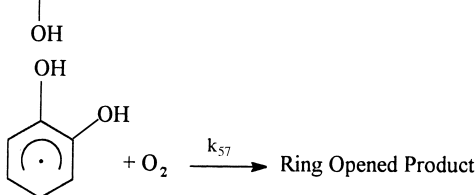
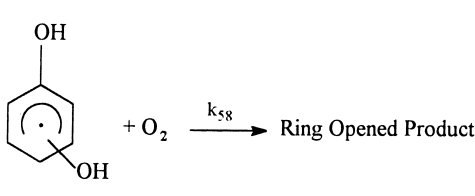
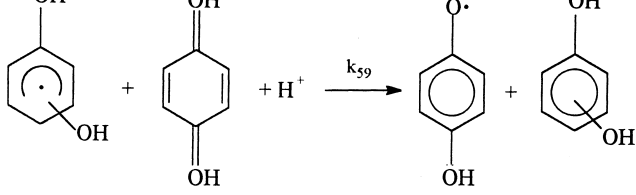
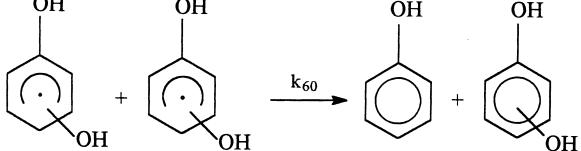
Reaction no.	Reaction
48	$O^{\bullet-} + O_2^{\bullet-} \xrightarrow{-k_{48}} 2OH^- + O_2$
49	$2HO_2^{\bullet} \xrightarrow{k_{49}} H_2O_2 + O_2$
50	$H^+ + OH^- \xrightarrow{k_{50}} H_2O$
51	$H^+ + HO_2^- \xrightarrow{k_{51}} H_2O_2$
52	$H_2O_2 \xrightarrow{k_{52}} H^+ + HO_2^-$
53	 <p>$\cdot OH + \text{Phenol} \xrightarrow{k_{53}} \text{Radical Intermediate}$</p>
54	 <p>$\cdot OH + \text{Hydroquinone} \xrightarrow{k_{54}} \text{Radical Intermediate}$</p>
55	 <p>$\text{Radical Intermediate} + H^+ \xrightarrow{k_{55}} \text{Semiquinone Radical} + H^+ + H_2O$</p>
56	 <p>$\text{Radical Intermediate} + H^+ \xrightarrow{k_{56}} \text{Semiquinone Radical} + H^+ + H_2O$</p>
57	 <p>$\text{Radical Intermediate} + O_2 \xrightarrow{k_{57}} \text{Ring Opened Product}$</p>
58	 <p>$\text{Radical Intermediate} + O_2 \xrightarrow{k_{58}} \text{Ring Opened Product}$</p>
59	 <p>$\text{Radical Intermediate} + \text{Hydroquinone} + H^+ \xrightarrow{k_{59}} \text{Semiquinone Radical} + \text{Semiquinone Radical}$</p>
60	 <p>$\text{Radical Intermediate} + \text{Radical Intermediate} \xrightarrow{k_{60}} \text{Phenol} + \text{Phenol}$</p>

Table 1 (Continued)

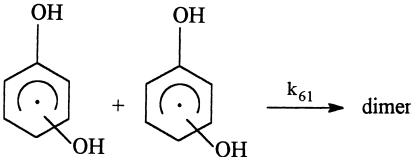
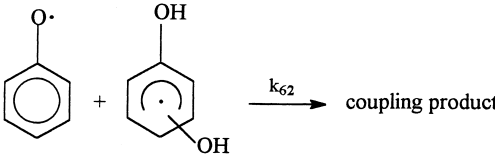
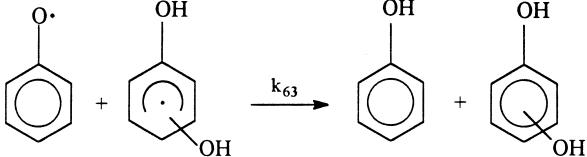
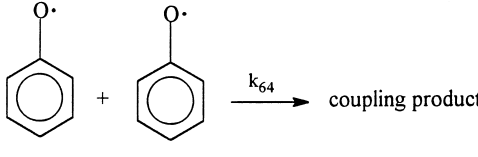
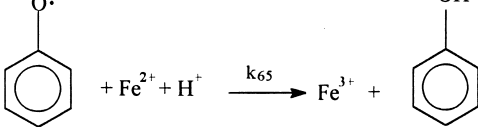
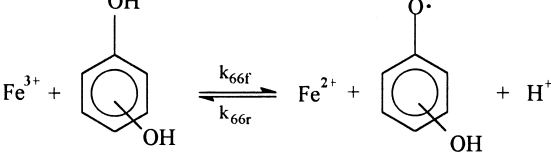
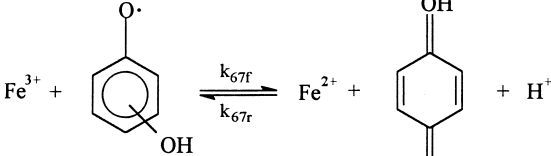
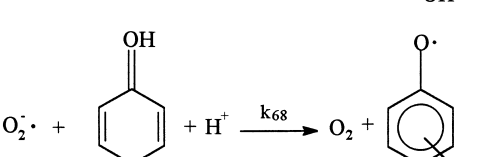
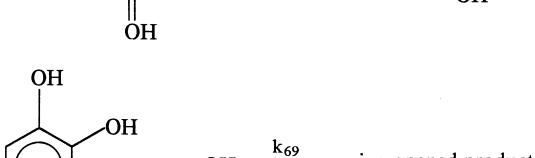
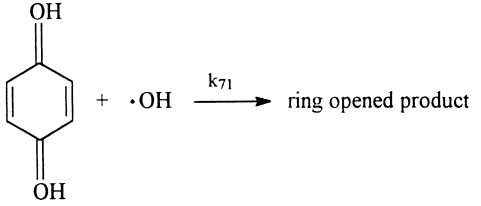
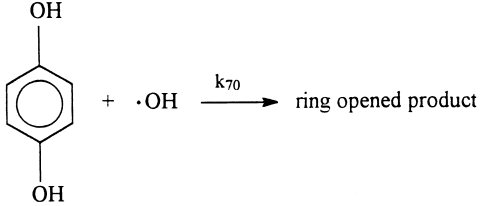
Reaction no.	Reaction
61	 $ \text{C}_6\text{H}_2(\text{OH})_4\cdot + \text{C}_6\text{H}_2(\text{OH})_4\cdot \xrightarrow{k_{61}} \text{dimer} $
62	 $ \text{C}_6\text{H}_2(\text{OH})_4\cdot + \text{C}_6\text{H}_2(\text{OH})_4\cdot \xrightarrow{k_{62}} \text{coupling product} $
63	 $ \text{C}_6\text{H}_2(\text{OH})_4\cdot + \text{C}_6\text{H}_2(\text{OH})_4\cdot \xrightarrow{k_{63}} \text{C}_6\text{H}_2(\text{OH})_4 + \text{C}_6\text{H}_2(\text{OH})_4\cdot $
64	 $ \text{C}_6\text{H}_2(\text{OH})_4\cdot + \text{C}_6\text{H}_2(\text{OH})_4\cdot \xrightarrow{k_{64}} \text{coupling product} $
65	 $ \text{C}_6\text{H}_2(\text{OH})_4\cdot + \text{Fe}^{2+} + \text{H}^+ \xrightarrow{k_{65}} \text{Fe}^{3+} + \text{C}_6\text{H}_2(\text{OH})_4 $
66	 $ \text{Fe}^{3+} + \text{C}_6\text{H}_2(\text{OH})_4\cdot \xrightleftharpoons[k_{66r}]{k_{66f}} \text{Fe}^{2+} + \text{C}_6\text{H}_2(\text{OH})_4\cdot + \text{H}^+ $
67	 $ \text{Fe}^{3+} + \text{C}_6\text{H}_2(\text{OH})_4\cdot \xrightleftharpoons[k_{67r}]{k_{67f}} \text{Fe}^{2+} + \text{C}_6\text{H}_2(\text{OH})_4 + \text{H}^+ $
68	 $ \text{O}_2\cdot + \text{C}_6\text{H}_2(\text{OH})_4\cdot + \text{H}^+ \xrightarrow{k_{68}} \text{O}_2 + \text{C}_6\text{H}_2(\text{OH})_4\cdot $
69	 $ \text{C}_6\text{H}_2(\text{OH})_4\cdot + \cdot\text{OH} \xrightarrow{k_{69}} \text{ring opened product} $

Table 1 (Continued)

Reaction no.	Reaction
70	 $\text{p-quinone} + \cdot\text{OH} \xrightarrow{k_{71}} \text{ring opened product}$
71	 $\text{hydroquinone} + \cdot\text{OH} \xrightarrow{k_{70}} \text{ring opened product}$

whereby hydrogen peroxide reacts with ferric or ferrous iron to produce hydroxyl radicals (see reaction (5) in Table 1). Furthermore, Sharma [25] showed that there was a specific level of iron that led to optimal phenol degradation.

Joshi et al. [26] measured the rates of formation of hydrogen peroxide (by direct chemical means) and hydroxyl radicals (by indirect chemical means) in liquid phase pulsed corona reactors. It was found that both rates were zero order, and that the reaction rate constants depended upon the magnitude of the applied electric field following the theory of Kuskova [27]. Joshi et al. [26] also developed a preliminary model of the reactions occurring in the pulsed corona reactor by combining experimental measurements of the rates of formation of hydrogen peroxide and hydroxyl radicals with known reactions from the radiation chemistry literature [28].

Sato and coworkers [11,29,30] and Sunka et al. [9] measured the formation of hydroxyl and other radicals and hydrogen peroxide by emissions spectroscopy, and they found similar results to those of Sharma et al. [8] for the degradation of phenol and the formation of reaction products. The general conclusion from these studies is that compounds such as phenol are primarily (but not solely) degraded through direct hydroxyl radical attack in a manner similar to other advanced oxidation technologies, and that hydroxyl radicals are generated by both direct formation and Fenton's reactions from hydrogen peroxide.

The critical reaction in the Fenton's chemistry is the catalysis of the formation of hydroxyl radicals from hydrogen peroxide and iron (see reaction (5) in Table 1). Fenton's reactions have been extensively studied for application to the degradation of a wide range of organic compounds including herbicides and pesticides [31–36], dyes [37], chlorinated phenols [38], and formaldehyde [39]. Fenton's reactions have been utilized in combination with UV/TiO₂ photocat-

alysts [40] and ultrasound [41]. The basic Fenton's reaction chemistry, including the general reaction mechanisms and kinetics of the major reactions for the degradation of phenol and other organic compounds, has been well studied.

Since it is clear that significant reactions of hydrogen peroxide and iron utilizing Fenton's reactions occur in the pulsed corona discharge reactor, it is important to develop quantitative models to describe the magnitude of the contribution of hydrogen peroxide to the degradation process. This is significant from a practical standpoint for the design, analysis, and control of the reactor [42]. It is also important to understand from the fundamental viewpoint the basic bulk phase chemical reactions in order to assess the relative contributions of other mechanisms, such as UV light [10] and shock wave-induced reactions, as well as potential surface-catalytic reactions [43], on the degradation processes.

The present study considers in detail the reactions occurring in the liquid phase pulsed corona reactor in the presence of iron salts. Specifically, a mathematical model describing the reactions occurring in the liquid phase pulsed corona reactor is developed by incorporating information from the literature on Fenton's reactions within the general framework of liquid phase corona reactor models. The pulsed corona reactor model utilizes basic reactions from the radiation chemistry literature as well as the same approach previously developed for liquid phase corona discharge [26]. Experimental measurements to determine the effects of salt concentration on the rates of formation of hydrogen peroxide are performed, and the results are incorporated within the model. Model predictions and model-data comparison are also presented, and the implications for reactor operation and design are discussed. A parametric sensitivity analysis is presented, detailing the important chemical reactions in the system.

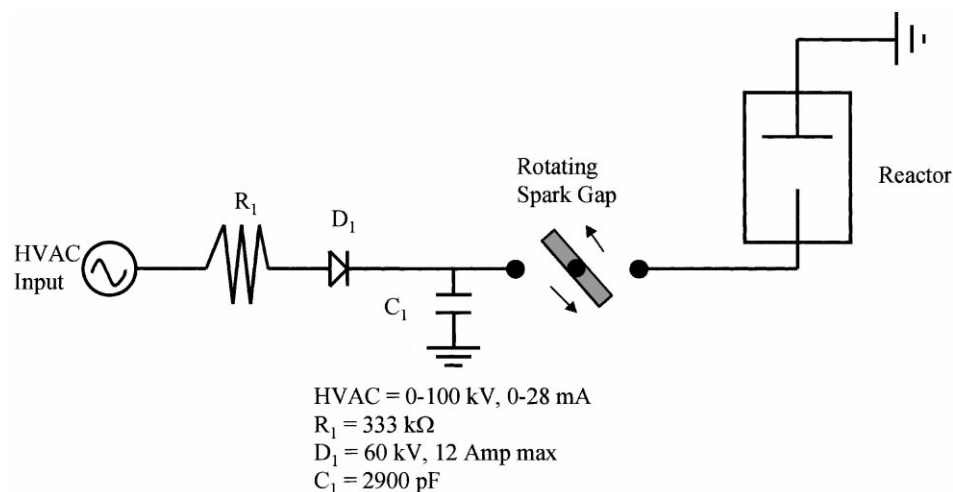


Fig. 1. Pulsed power supply circuit diagram.

2. Materials and methods

The power supply used in the present study is identical to that used in previous work [8,26,43] and is shown in Fig. 1. The high voltage alternating input current first goes through a series of high voltage current limiting resistors. A series of diodes is used to half-wave rectify the alternating current. The current is then stored in a bank of capacitors that are connected to a rotating spark gap. When a rotating rod (1800 rpm) in the spark gap aligns with two opposing copper electrodes (one attached to the capacitors and one attached to the reactor), the charge stored in the capacitors is discharged across the gap resulting in a pulsed discharge delivered into the liquid phase reactor. The rotating rod in the spark gap aligns with the two copper electrodes twice for each full rotation, thus leading to an alignment frequency of 60 Hz.

The pulsed corona reactor used in the present study is also similar to that used in previous research [43] and is shown in Fig. 2. The reactor consists of a 1 l glass chamber with a water jacket for temperature control. Cooling water flowed through the jacket at a temperature of 20.0°C which provide sufficient cooling to maintain the reactor at this temperature as measured before and after each experiment. A glass tube on the side of the reactor was used to insert the high voltage lead into the reactor. A glass cap with a mechanically sharpened 1 mm diameter platinum wire was attached to the end of the glass tube. This point electrode was electrically connected to the output from the spark gap. The stainless steel ground plane electrode is located 5 cm above the point electrode. This ground electrode is attached to ground. Corona generated at the tip of the point electrode extends upward toward the stainless steel ground plate, forming a non-uniform point-to-plane electrode geometry. The discharge region is roughly hemispherical in shape between the two electrodes. A magnetic stirring bar at the bottom of the reactor was used

to keep the solution well mixed. Three open ports on the lid of the reactor were used for taking liquid samples during the experiments.

Measurements of the applied voltage and current waveforms were made for all experimental trials. Peak voltage, rise time, and pulse width were measured by placing a Tektronix P6015A high voltage probe coupled to a Tektronix TDS 460 fast digital storage oscilloscope in parallel with the ground of the input of the pulsed power to the reactor. Reactor current was measured with a P6021 Tektronix current probe, and the reactor electric power was calculated by integration of the product of voltage and current using the Wavestar program from Tektronix. Typical voltage and current waveforms are shown in Fig. 3. As indicated, the expected voltage pulse has a very fast rise time (in the order of 20 ns), and then an exponential decay. The voltage pulse width is dependent on the conductivity of the solution in the reactor, and is in the range of 1 μs to 1 ms.

The chemicals used throughout the study included potassium chloride, ferrous sulfate, phenol, resorcinol, hydroquinone, catechol, acetic acid, and acetonitrile (all obtained from Fisher Scientific). All chemicals were used as received from the manufacturer. Deionized water was available with a conductivity of less than 1 $\mu\text{S}/\text{cm}$. Three or more trials were performed for most sets of experimental conditions, and averages of these data are reported (all data reported had errors of less than 5%). Initial and final measurements of conductivity (Cole-Parmer Model 1484-10 conductivity meter), pH (Fisher Accumet 950 pH meter), and temperature (standard mercury thermometer) were obtained. A Perkin-Elmer HPLC was used to analyze the organic species in the solutions. Samples were analyzed using a Supelco Supercosil C18 column (25.0 cm \times 4.6 mm) with a mobile phase of 0.5% acetic acid, 5.0% acetonitrile, and 94.5% deionized water. The flow rate of the mobile phase was 1.0 ml/min. A Perkin-Elmer Spectrophotometer LC80 was coupled to the

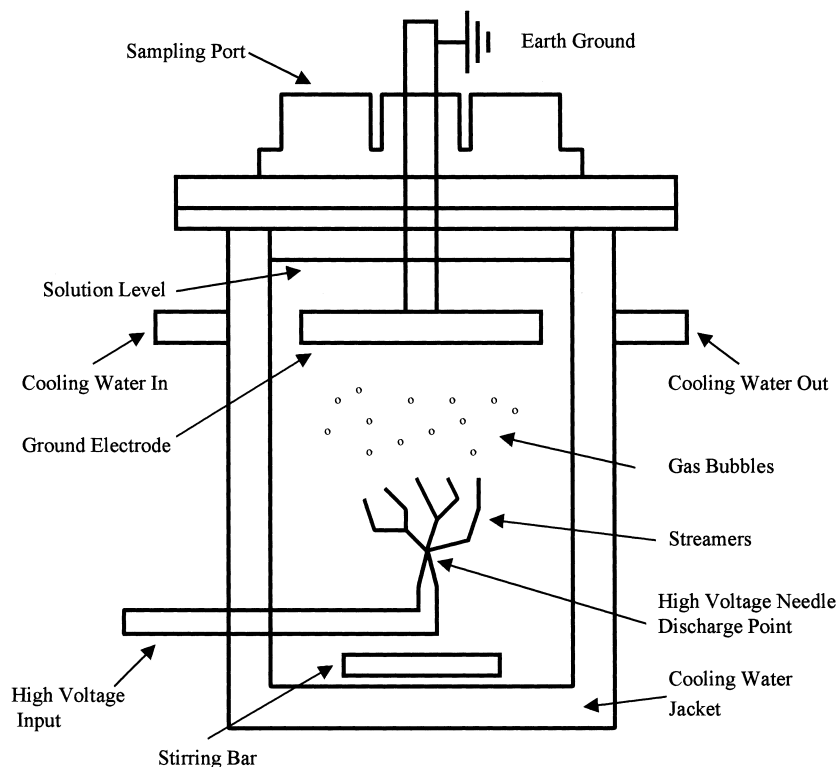


Fig. 2. Schematic of jacketed liquid phase pulsed corona reactor.

HPLC at a wavelength of 280 nm. The recorded peaks were identified and quantified from a set of calibration standards of phenol and the primary oxidation by-products including catechol, hydroquinone and resorcinol.

The rates of hydrogen peroxide formation as a function of solution conductivity were determined at two applied voltages (46 and 57 kV peak voltage) for solutions without phenol or iron salts. Experimental trials were performed with initial solution conductivities ranging from 7 to 600 $\mu\text{S}/\text{cm}$

using potassium chloride. Samples were analyzed for hydrogen peroxide using the method developed by Ghormoley [44,45].

Experimental trials were performed to determine the effects of Fe^{2+} concentration on the phenol removal rate. These experiments were performed with 10 ppm initial phenol concentration in deionized water, and various Fe^{2+} concentrations ranging from 24 to 1968 μM FeSO_4 solutions. These experiments were conducted using a corona

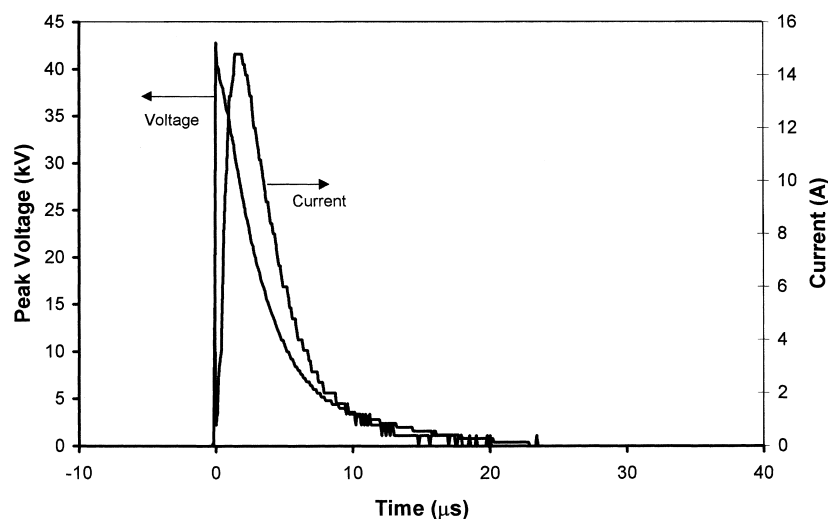


Fig. 3. Current and voltage waveforms for 150 $\mu\text{S}/\text{cm}$ KCl solution.

discharge with a peak voltage of 46 kV. Phenol degradation and by-product formation in solutions with an initial 100 ppm phenol concentration at an applied peak voltage of 57 kV were also performed with a single initial solution conductivity of 150 $\mu\text{S}/\text{cm}$ arising from a FeSO_4 concentration of 485 μM .

3. Model formulation

Initial models of the bulk phase corona-induced chemical reactions were reported by Joshi et al. [26]. In that study, it was assumed that the pulsed corona discharge leads to the formation of hydrogen peroxide, hydroxyl radicals, and aqueous electrons through reactions (1)–(3) as shown in Table 1. These rate constants depended on the operating variables of the reactor, such as peak voltage, electrode gap spacing, and conductivity. The other major species produced by the corona reactor were assumed to be the same as those formed in radiation processes such as electron beam irradiation and pulsed radiolysis, as indicated by the propagation and termination reactions (reactions (4)–(52)) given in Table 1. The reactions involving the various organic species are given by reactions (53)–(71). The oxidation reactions for the organic compounds, in this case phenol and its primary oxidation products, were assumed to follow the kinetics of liquid phase hydroxyl radical attack as given by reactions (53)–(54) and (69)–(71) in Table 1.

The present study utilizes the basic reactions reported by Joshi et al. [26] and the reaction scheme reported by Chen and Pignatello [46], supplemented with the addition of the various radiation chemistry and iron reactions that lead to hydrogen peroxide decomposition. The kinetic rate constants for most of these reactions were obtained from the radiation and oxidation chemistry literature, and were chosen to correspond to similar temperature and pH conditions as in the present study. The values of the reaction rate constants are given in Table 2, and their sources are the following:

k_4	[47]
k_5 and k_6	[23]
k_7, k_8, k_9 and k_{10}	[48]
k_{11}	[49]
k_{12}	[50]
$k_{13}, k_{21}, k_{23}, k_{27}, k_{29}, k_{31},$ $k_{36}, k_{38}, k_{42}, k_{45},$ k_{47}, k_{53} and k_{54}	[51]
$k_{14}, k_{15}, k_{16}, k_{17}, k_{49}, k_{69}$	[51]
k_{18}	[52]
k_{19} and k_{20}	[53]
k_{22}	[54]
k_{24}	[55]
k_{25}	[56]
k_{26} and k_{32}	[57]
k_{28}	[58]

k_{30}	[59]
k_{33}	[60]
k_{34} and k_{35}	[61]
k_{37} and k_{40}	[62]
k_{39}	[63]
k_{41}	[64]
k_{46} and k_{48}	[65]
k_{55}, k_{56} and k_{59}	[66]
$k_{57}, k_{58}, k_{62}, k_{63}, k_{65}$ and k_{67r}	[46]
k_{60} and k_{61}	[67]
k_{64} and k_{68}	[68]
k_{66f} and k_{66r}	[69]
k_{67f}	[70]

The initiation reactions, reactions (1)–(3) given in Table 1, are assumed to be the only reactions directly associated with the pulsed streamer corona. The rate constants for reactions (1) and (3) in the present study are assumed to be the same as those determined by Joshi et al. [26]. The rate constant for reaction (2) was fit to data from experiments reported in the present paper on hydrogen peroxide formation (in the absence of iron salts and phenol) in the pulsed corona reactor. The present studies indicate a somewhat larger rate of formation of hydrogen peroxide in the pulsed corona reactor than was found by Joshi et al. [26]. This difference may be partially attributed to some modifications in the reactor, including, in the present work, the use of platinum rather than stainless steel high voltage electrodes. The propagation and termination reactions (reactions (4)–(53)), as well as the organic reactions (53)–(71), are assumed to be

Table 2

Reaction rate constants ($\text{M}^{-1} \text{s}^{-1}$) for reactor model

$k_1 = 9.25 \times 10^{-10}$	$k_{26} = 3.4 \times 10^{10}$	$k_{51} = 2.6 \times 10^{10}$
$k_2 = 2.0 \times 10^{-6}$	$k_{27} = 5.5 \times 10^9$	$k_{52} = 3.7 \times 10^{-2}$
$k_3 = 2.35 \times 10^{-9}$	$k_{28} = 1.3 \times 10^{10}$	$k_{53} = 7.0 \times 10^9$
$k_4 = 0.01$	$k_{29} = 1.9 \times 10^{10}$	$k_{54} = 0.3 \times 10^9$
$k_5 = 76$	$k_{30} = 1.3 \times 10^{10}$	$k_{55} = 1.0 \times 10^8$
$k_6 = 4.3 \times 10^8$	$k_{31} = 2.3 \times 10^{10}$	$k_{56} = 1.0 \times 10^9$
$k_7 = 1.0 \times 10^4$	$k_{32} = 1 \times 10^{-3}$	$k_{57} = 1.5 \times 10^9$
$k_8 = 1.2 \times 10^6$	$k_{33} = 3.5 \times 10^9$	$k_{58} = 1.5 \times 10^9$
$k_9 = 1.5 \times 10^8$	$k_{34} = 3.0 \times 10^{10}$	$k_{59} = 3.7 \times 10^9$
$k_{10} = 1.0 \times 10^7$	$k_{35} = 2.2 \times 10^{10}$	$k_{60} = 5.0 \times 10^8$
$k_{11} = 6.0 \times 10^{10}$	$k_{36} = 1.2 \times 10^{10}$	$k_{61} = 5.0 \times 10^8$
$k_{12} = 2.0 \times 10^6$	$k_{37} = 2.0 \times 10^{10}$	$k_{62} = 5.0 \times 10^8$
$k_{13} = 2.7 \times 10^7$	$k_{38} = 5.0 \times 10^9$	$k_{63} = 5.0 \times 10^8$
$k_{14} = 8.0 \times 10^{-5}$	$k_{39} = 7.0 \times 10^9$	$k_{64} = 1.0 \times 10^9$
$k_{15} = 5.0 \times 10^{10}$	$k_{40} = 2.0 \times 10^{10}$	$k_{65} = 1.0 \times 10^5$
$k_{16} = 8.5 \times 10^5$	$k_{41} = 5.0 \times 10^7$	$k_{66f} = 4.4 \times 10^2$
$k_{17} = 9.7 \times 10^7$	$k_{42} = 2.2 \times 10^7$	$k_{66r} = 1.1 \times 10^3$
$k_{18} = 3.9 \times 10^7$	$k_{43} = 1.0 \times 10^{10}$	$k_{67f} = 4.4 \times 10^4$
$k_{19} = 1 \times 10^{10}$	$k_{44} = 9.4 \times 10^{-7}$	$k_{67r} = 1.2 \times 10^{-3}$
$k_{20} = 1 \times 10^{10}$	$k_{45} = 4.0 \times 10^8$	$k_{68} = 1.0 \times 10^9$
$k_{21} = 5.5 \times 10^9$	$k_{46} = 8.0 \times 10^7$	$k_{69} = 1.1 \times 10^{10}$
$k_{22} = 1.3 \times 10^{10}$	$k_{47} = 4.0 \times 10^8$	$k_{70} = 5.0 \times 10^9$
$k_{23} = 2.7 \times 10^7$	$k_{48} = 6.0 \times 10^8$	$k_{71} = 1.2 \times 10^9$
$k_{24} = 2.0 \times 10^{10}$	$k_{49} = 8.3 \times 10^5$	
$k_{25} = 7.5 \times 10^9$	$k_{50} = 1.4 \times 10^{11}$	

independent of the pulsed corona discharge. The rate constants in reactions (4)–(52) are taken from the radiation chemistry literature.

Since the pulsed corona reactor is known to produce significant quantities of hydrogen peroxide, it is useful to add iron salts to enhance hydroxyl radical formation and thus organic contaminant degradation. The important steps in the reaction mechanism are the iron reactions (reactions (4)–(12) and (65)–(67) in Table 1) where the main reaction is reaction (5). This reaction consumes Fe^{2+} while reacting with the hydrogen peroxide to form the hydroxyl radical. Several of the other iron reactions involve the regeneration of the ferrous ion by various means. The reactions necessary to accomplish this regeneration are reactions (66) and (67) shown in Table 1. These two reactions involve reactions between Fe^{3+} and either hydroquinone, catechol, or the semiquinone radical. Once hydroquinone and catechol are formed, the Fe^{2+} is regenerated, thereby resulting in continuous cycling between Fe^{2+} and Fe^{3+} . Further discussion of these reactions is found in Chen and Pignatello [46].

Phenol is a suitable representative small aromatic compound because its oxidation has been extensively studied in a number of systems. These include treatment by supercritical water oxidation [71–73], ultrasonication [74], ozonation [75,76], UV photolysis [32,35], and pulsed streamer corona [25]. In most of these studies, the oxidation of phenol was achieved through reaction with hydroxyl radicals. Hydroxyl radicals electrophilically attack phenol to form the primary products catechol, resorcinol, and hydroquinone. Other hydroxyl radicals then react with these primary products to produce muconic and fumaric acids as well as other organic acids. These organic acids are then oxidized to form the smaller organic acids such as oxalic and formic acids. The final end products of the hydroxyl radical oxidation of phenol are carbon dioxide and water [73,77]. In the present study only the first few oxidation reactions are considered in the model. It is useful to note that recent studies have considered a wide range of by-product formation in the case of corona discharge produced with the high voltage electrode placed above the surface of water and the ground electrode placed within the water [78].

The general mass balance for a well-mixed, constant volume, and constant temperature batch reactor is given by

$$\frac{dc_i}{dt} = -r_i \quad (1)$$

where c_i is the average concentration in the bulk solution of species i , and r_i is the bulk phase rate of formation of that species. A total of 31 simultaneous ordinary differential equations were solved using a Gear routine by Mathematica Version 3.0 (from Wolfram Research, Champaign, IL). The initial iron concentration ranged from 24 to 1936 μM , with the most typical value of 485 μM . The initial concentration of phenol was either 10 or 100 ppm. The other initial conditions included a pH value of 5, a dissolved oxygen concentration of 250 μM [46], and other species were not present.

In order to determine the sensitivity of the model output to input reaction rate constants and the importance of specific reactions, a parametric sensitivity analysis, as described by Varma et al. [79], is used. The system of chemical reactions is represented by a vector y with n components, and is determined by solution of the differential equations

$$\frac{dy_i}{dt} = f_i(y, \phi, t) \quad (2)$$

with initial conditions

$$y_i(0) = y_i^i \quad (3)$$

where y_i is the dependent variable, t the time, and ϕ is the vector containing m system input variables. For the kinetic model used in the present study, y_i is the average concentration in the bulk phase of species i , and ϕ is the vector of reaction rate constants. The general solution to Eq. (2) is

$$y_i = y_i(t, \phi) \quad (4)$$

The sensitivity coefficients, $s(y_i; \phi_j)$, determine how a small change in one reaction rate constant, or in general any model parameter, affects the dependent variables and are defined by

$$s(y_i; \phi_j) = \frac{\partial y_i(t, \phi_j)}{\partial \phi_j} \quad (5)$$

Normalized sensitivity coefficients are defined as

$$S(y_i; \phi_j) = \left(\frac{\phi_j}{y_i} \right) s(y_i; \phi_j) \quad (6)$$

For the current kinetic system, the following equations are solved simultaneously with the system ordinary differential equations representing the material balances:

$$\frac{ds_j}{dt} = \underline{J}(t)s_j + \frac{\partial \underline{f}(t)}{\partial \phi_j} \quad (7)$$

with initial conditions

$$s(y_i; \phi_j)|_{t=0} = \begin{cases} 0, & \phi_j \neq y_j^i \\ 1, & \phi_j = y_j^i \end{cases} \quad (8)$$

where

$$\underline{J}(t) = \frac{\partial \underline{f}}{\partial y} = \begin{bmatrix} \frac{\partial f_1}{\partial y_1} & \frac{\partial f_1}{\partial y_2} & \cdots & \frac{\partial f_1}{\partial y_n} \\ \frac{\partial f_2}{\partial y_1} & \frac{\partial f_2}{\partial y_2} & \cdots & \frac{\partial f_2}{\partial y_n} \\ \vdots & \vdots & \ddots & \vdots \\ \frac{\partial f_n}{\partial y_1} & \frac{\partial f_n}{\partial y_2} & \cdots & \frac{\partial f_n}{\partial y_n} \end{bmatrix} \quad (9)$$

and

$$\frac{\partial f(t)}{\partial \phi_j} = \begin{bmatrix} \frac{\partial f_1}{\partial \phi_j} \\ \frac{\partial f_2}{\partial \phi_j} \\ \vdots \\ \frac{\partial f_n}{\partial \phi_j} \end{bmatrix} \quad (10)$$

4. Results and discussion

The effect of aqueous solution conductivity on the rate of hydrogen peroxide formation is shown in Fig. 4 for two different pulsed corona operating voltages. The results for the 46 kV (peak voltage) experiments show an increase of hydrogen peroxide formation as the solution conductivity decreases from 600 to 7 $\mu\text{S}/\text{cm}$. For the case of 150 $\mu\text{S}/\text{cm}$ solution conductivity, the energy per pulse was 730 mJ per pulse, corresponding to a hydrogen peroxide production efficiency of 1.0 g/kWh. The solution having the lowest conductivity, the 7 $\mu\text{S}/\text{cm}$ potassium chloride solution, gave the highest hydrogen peroxide production rate with an energy of 380 mJ per pulse, leading to a hydrogen peroxide production efficiency of 3.64 g/kWh. For the 57 kV (peak voltage) experiments, electrical breakdown occurred below a conductivity of 150 $\mu\text{S}/\text{cm}$ and the corona became intermittent above 350 $\mu\text{S}/\text{cm}$. The experiments at 57 kV also showed a smooth decrease in hydrogen peroxide formation rate with conductivity in the range of 150–350 $\mu\text{S}/\text{cm}$. The total drop in hydrogen peroxide formation over this conductivity range was about 40% for the higher voltage case. This reduction in

hydrogen peroxide production with increasing conductivity parallels qualitative visual observations that show decreasing streamer length as conductivity is increased, thus implying that as the streamer length decreases the rate of formation of hydrogen peroxide also decreases. At the higher voltage and 150 mS/cm solution conductivity, the energy per pulse was 1496 μJ per pulse, corresponding to a hydrogen peroxide production efficiency of 1.56 g/kWh. These experimental results showing the effect of conductivity on hydrogen peroxide are consistent with other recent studies [80] where an exponential decrease in hydrogen peroxide formation rate with conductivity was found for conductivity from 100 to 500 $\mu\text{S}/\text{cm}$. However, it is also interesting to note that Lukes et al. [80] found in these recent studies that as the conductivity increases the formation of ultraviolet light by the plasma increases.

Experimental data showing the effects of iron concentration on the removal of phenol from a solution with an initial concentration of 10 ppm are shown in Fig. 5. At a very low iron concentration of 24 μM , very little phenol degradation occurs; however, as the iron concentration is increased to 485 μM the rate of phenol degradation increases dramatically. The experimental data also shows that as iron concentration is increased further, the rate of phenol degradation decreases. Thus, an optimal value, or range, of iron concentration occurs for phenol degradation.

Fig. 6 shows the model predictions of the effect of initial iron concentration on the rate of phenol removal for conditions (i.e. voltage, conductivity, pH, and initial iron and phenol concentrations) equivalent to those of the experiments shown in Fig. 5. The hydrogen peroxide production rates used in the simulations shown in Fig. 6 were taken from the experimental data, at equivalent solution conductivity, reported in Fig. 4. The model predicts an optimal iron concentration with respect to phenol removal, as seen in the

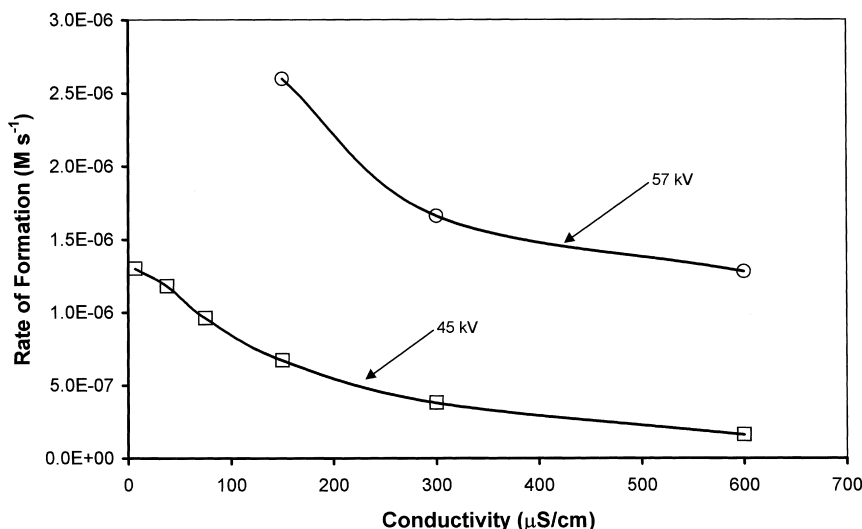


Fig. 4. Experimental results showing the effect of solution conductivity on hydrogen peroxide formation for two different corona treatment voltages.

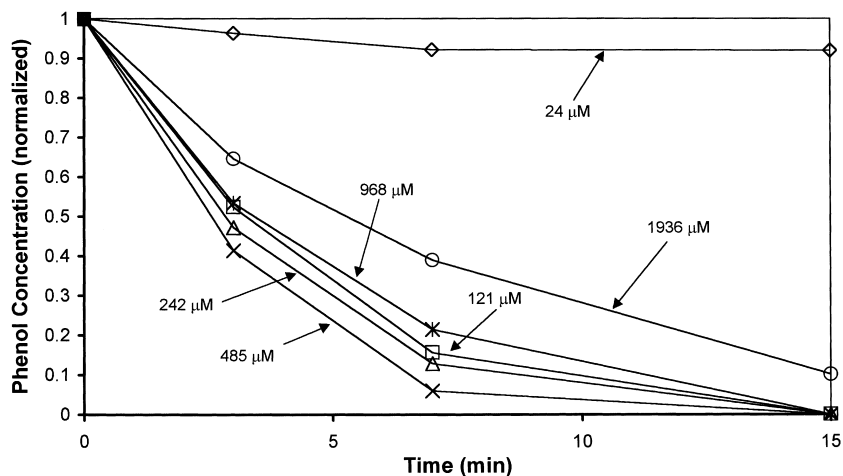


Fig. 5. Experimental results showing the effect of iron concentration on phenol degradation with 46kV pulsed corona treatment (initial phenol concentration = 10 ppm).

experiments; however, the model shows an optimal iron concentration in the range of 121–485 μM and the experiments show a value closer to 485 μM . The model shows little difference between the results for 121 and 242 μM , however, the results for 484 μM differ from the other two cases for times above approximately 4 min. While the experimental data for the iron concentrations of 121, 242, and 485 μM are fairly close to each other, the reproducibility of the measurements was very good and the experimental variability was less than 5%. The model also shows a slightly faster decay in phenol than seen in the experiments at the 24 μM concentration. However, for the 968 and 1936 μM concentrations the model shows a somewhat slower drop in phenol concentration than the experimental data. This might be explained by the occurrence of iron flocculation at the higher iron concentrations. At 968 and 1936 μM iron con-

centration, iron begins to flocculate out of solution, which would cause the iron concentration in solution to decrease. As seen in both the theoretical and experimental results, at a lower iron concentration, phenol removal would increase provided that the iron concentration would not drop to near zero. In addition, as mentioned above, Lukes et al. [80] found significant rates of production of ultraviolet light at high solution conductivity and Sun et al. [10] suggest that ultraviolet light may be important in the liquid phase pulsed corona process. It is therefore possible that at the higher conductivity other reaction processes (not included in the current model) involving ultraviolet light and other radical species may begin to come into play. These reactions could perhaps also affect the iron flocculation. Despite the quantitative differences between the experiments and the model, these results, in general, are very encouraging because the

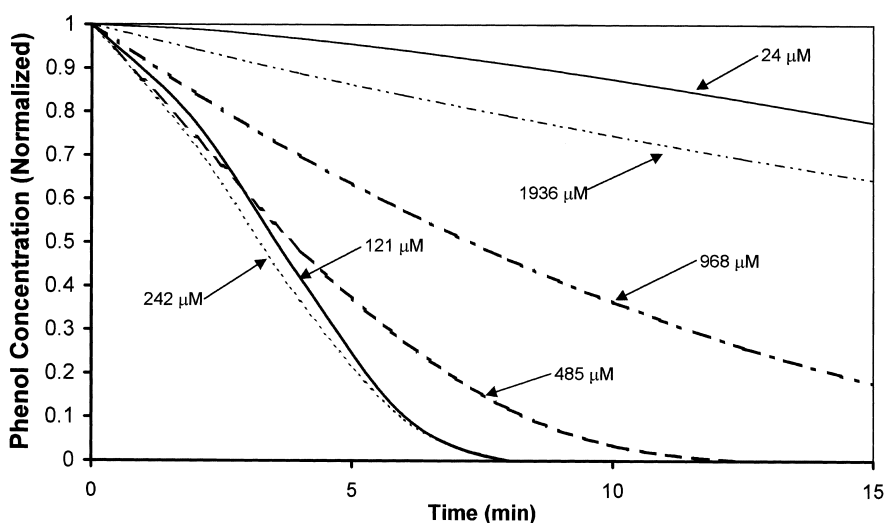


Fig. 6. Kinetic simulations showing the effect of iron concentration on phenol degradation with 46kV pulsed corona treatment (initial phenol concentration = 10 ppm).

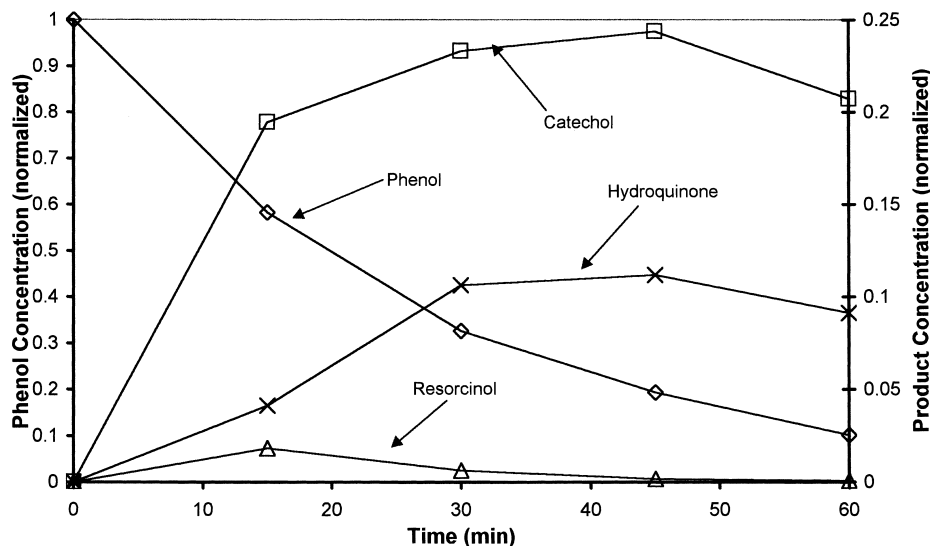


Fig. 7. Experimental results showing the phenol and major by-product concentrations for 57 kV pulsed corona treatment and 485 μM FeSO_4 (initial phenol concentration = 100 ppm).

model uses reaction rate parameters obtained by independent experiments conducted in our laboratory and from the literature. No model-data fitting was performed to assess the effects of iron concentration on the phenol removal.

Experimental data on phenol and primary by-product concentrations are shown in Fig. 7 for the case of a discharge with 57 kV peak voltage and 485 μM FeSO_4 . These results compare favorably with the model predictions shown in Fig. 8 (note that resorcinol is not included in the model). The phenol and catechol concentrations, in general, are well predicted by the model, although the model shows a larger drop in catechol concentration in the last few minutes of the experiment than is observed in the data. Further, the catechol and hydroquinone concentrations in the model are significantly less than those observed in the experiments. This result may also be due to the absence of additional hydroxyl

radical reactions with other by-products not included in the model, e.g. ring opened products, dimers, coupling products, etc.

Other model results for the same conditions shown in Fig. 8 are shown in Figs. 9–12. Fig. 9 shows the concentration of Fe^{2+} as a function of time for 60 min. The Fe^{2+} concentration decreases in the first few minutes, and thereafter rises to an approximately steady value until approximately 50 min, thenceforth it decreases a small amount. During the first 5 min, when the initial Fe^{2+} drop occurs, little hydroquinone and catechol are formed. After 5 min these species increase in concentration, leading to the regeneration of Fe^{2+} through reactions with catechol and hydroquinone as indicated by reaction (67) in Table 1. After 50 min Fe^{2+} decreases, corresponding to the decrease in hydroquinone and catechol at these times.

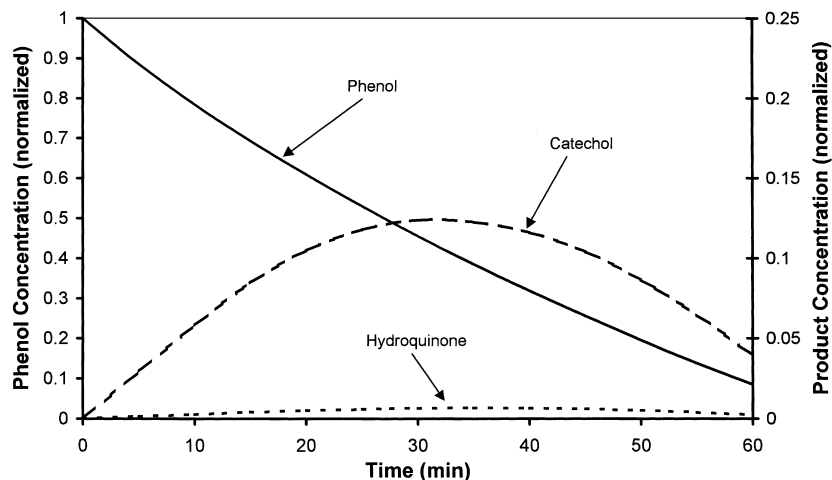


Fig. 8. Kinetic simulations showing phenol and by-product concentrations for 57 kV pulsed corona treatment and 485 μM FeSO_4 (initial phenol = 100 ppm).

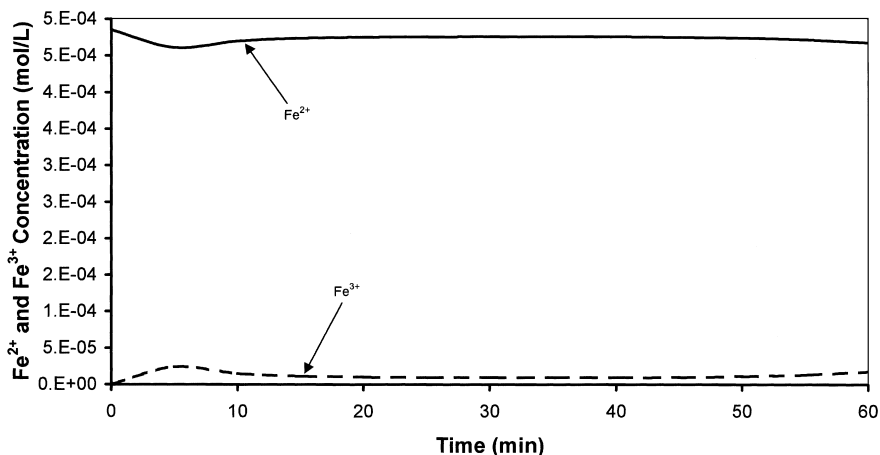


Fig. 9. Kinetic simulations showing Fe^{2+} and Fe^{3+} concentrations for 57 kV pulsed corona treatment and $485 \mu\text{M}$ FeSO_4 (initial phenol concentration = 100 ppm).

Fig. 10 shows that the model predicts a decrease in pH from the initial value of 5.0 to a relatively stable level of about 3.8 after about 10 min. This result is also very encouraging since experimental results, also included in the figure, show that the initial pH of 5.0 drops to about 3.8 in the first 15 min and remains steady up to 1 h. Hydrogen peroxide, shown in Fig. 11, is predicted to reach a steady-state value of about $1 \times 10^{-5} \text{ M}$ in the first 10 min.

Aqueous electron concentration plotted versus time in Fig. 12 shows a concentration time course similar to that of hydrogen peroxide, albeit reaching a much lower steady-state concentration of 10^{-16} M . Hydroxyl radical (ca. 10^{-13} M) and hydrogen radical (ca. 10^{-18} M) concentrations show similar small, but rapid, changes in concentrations within the first 10 min of the run, followed by larger but slower changes for times up to 60 min. Peroxyhydroxyl radical (HO_2 , ca. 10^{-12} M) and O_2^- (ca. 10^{-11} M) show similar increases in concentration during the first 10 min, reaching peak values at approximately 5 min, followed by

long steady decreases during the rest of the 60 min time period.

Figs. 13–15 show model predictions for the case of 57 kV peak voltage and $485 \mu\text{M}$ ferrous sulfate when no phenol is present. Fig. 13 shows the Fe^{2+} and Fe^{3+} concentrations as functions of time. The Fe^{2+} is depleted from the solution in approximately 15 min and is not regenerated for the duration of the simulation. This is due to the absence of phenol in the solution, thereby preventing the formation of catechol and hydroquinone. With these species absent, reaction (66) in Table 1 does not occur, and therefore none of the Fe^{3+} can be converted back to Fe^{2+} .

After the Fe^{2+} is depleted from the system, Fenton's reaction does not occur and hydrogen peroxide steadily increases, as shown in Fig. 14. During early times of the simulation, when Fe^{2+} is still present, hydrogen peroxide is consumed at a high rate, but after all of the Fe^{2+} is consumed, the hydrogen peroxide increases at an almost linear rate. Fig. 15 shows the radical concentrations as functions of

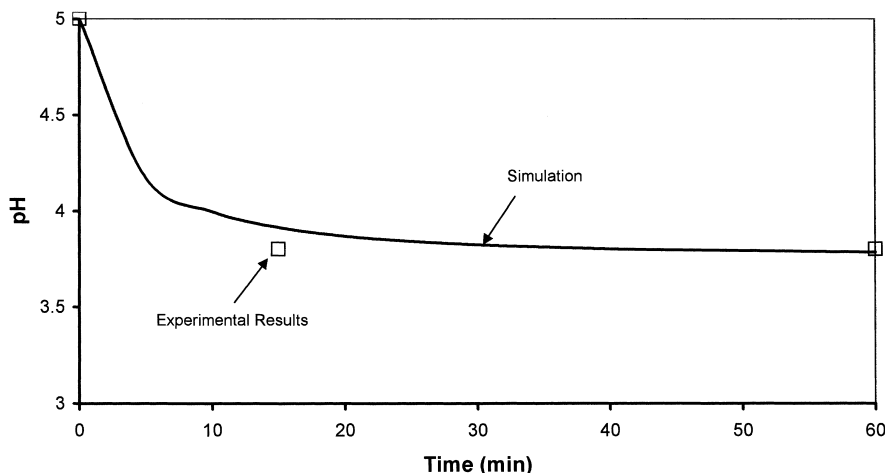


Fig. 10. Kinetic simulations showing pH variation for 57 kV pulsed corona treatment and $485 \mu\text{M}$ FeSO_4 (initial phenol concentration = 100 ppm).

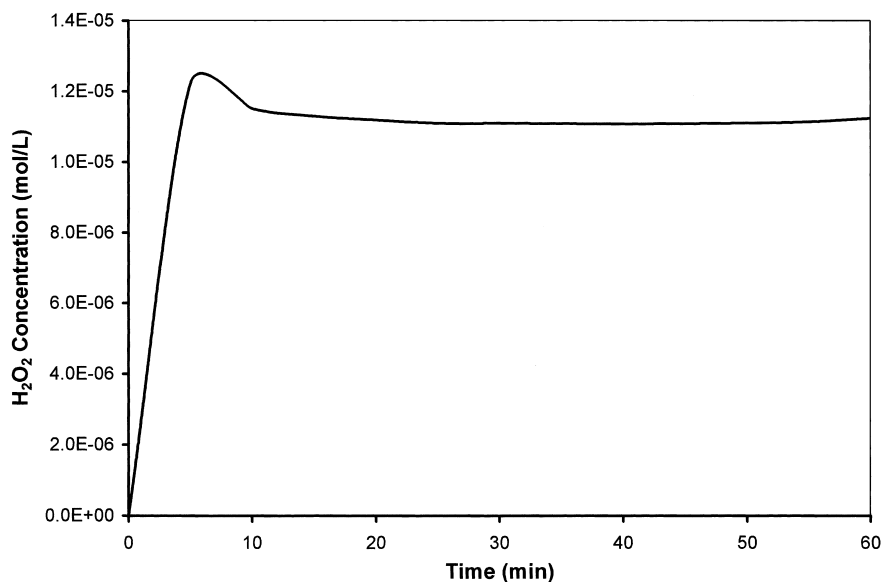


Fig. 11. Kinetic simulations showing hydrogen peroxide concentration for 57 kV pulsed corona treatment and 485 μM FeSO_4 (initial phenol concentration = 100 ppm).

time for this case. Hydroxyl radical concentrations are two orders of magnitude higher (10^{-11} M) for the case without phenol compared to the case with phenol. This is simply due to the lack of organic molecules to consume the hydroxyl radicals in the latter case.

Fig. 16 shows the model predictions for the case of phenol removal at high initial phenol concentration (i.e. 100 ppm) for different concentrations of iron salt. The iron salt concentration is varied over a very large range (0.1 – 10^{-5} M) to illustrate the level of optimal concentration. The general trends are very similar to those where the initial phenol concentration was 10 ppm as shown in Fig. 6. However, at the higher initial concentration, the phenol removal is less sensitive to the iron concentration, as indicated by phenol removal values that are similar for initial iron concentrations

in the range of 10^{-3} – 10^{-4} M. Note that the results shown in Fig. 16 do not account for variations in the hydrogen peroxide rate of formation with conductivity. These results would therefore correspond to cases where other non-iron containing salts, e.g. potassium chloride, would be added to the system to give the same starting conductivity.

Fig. 17 shows the effects of iron concentration with different rates of hydrogen peroxide formation (due to solution conductivity changes) for the model simulation of phenol removal at high initial phenol concentration. As shown in Fig. 17, at the 485, 968, and 1451 μM ferrous sulfate concentrations, the amounts of phenol removed in 60 min are virtually identical when the hydrogen peroxide production rates are assumed to be the same. When the rates of production of hydrogen peroxide are adjusted to those shown in

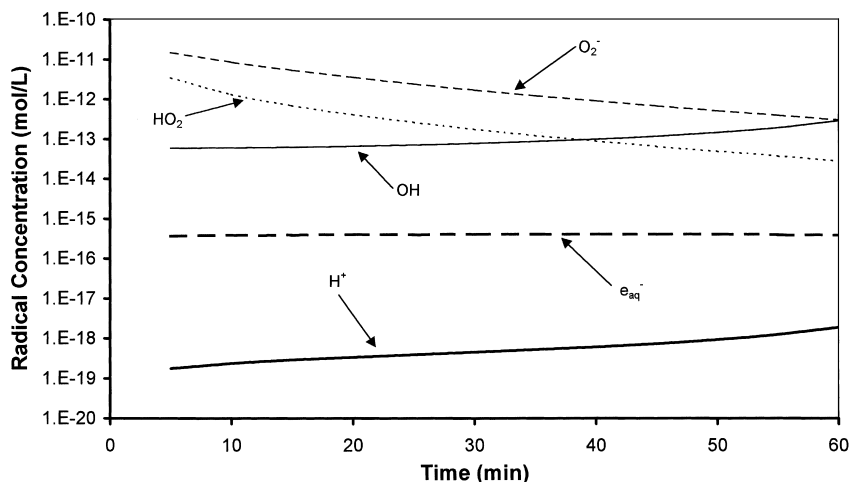


Fig. 12. Kinetic simulations showing radical concentrations for 57 kV pulsed corona treatment and 485 μM FeSO_4 (initial phenol concentration = 100 ppm).

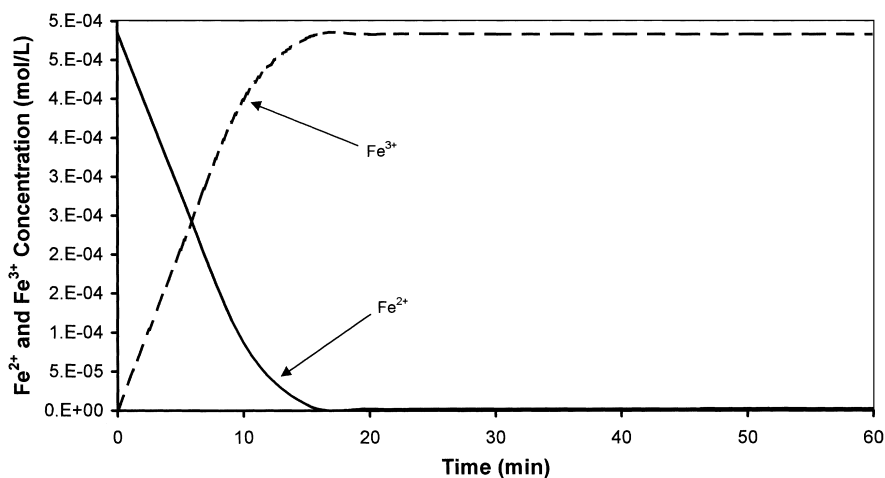


Fig. 13. Kinetic simulations showing Fe^{2+} and Fe^{3+} concentrations for 57 kV pulsed corona treatment and $485 \mu\text{M}$ FeSO_4 (initial phenol = 0 ppm).

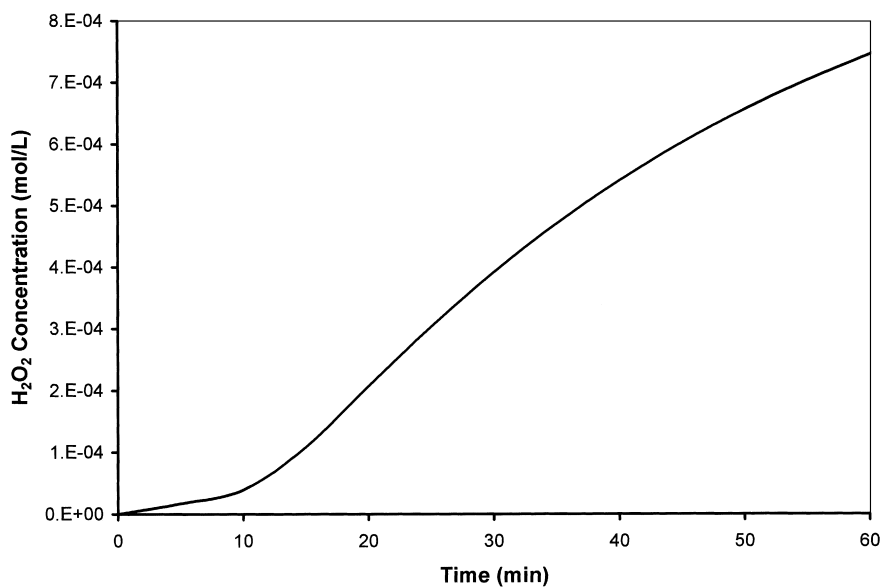


Fig. 14. Kinetic simulations showing hydrogen peroxide concentration for 57 kV pulsed corona treatment and $485 \mu\text{M}$ FeSO_4 (initial phenol = 0 ppm).

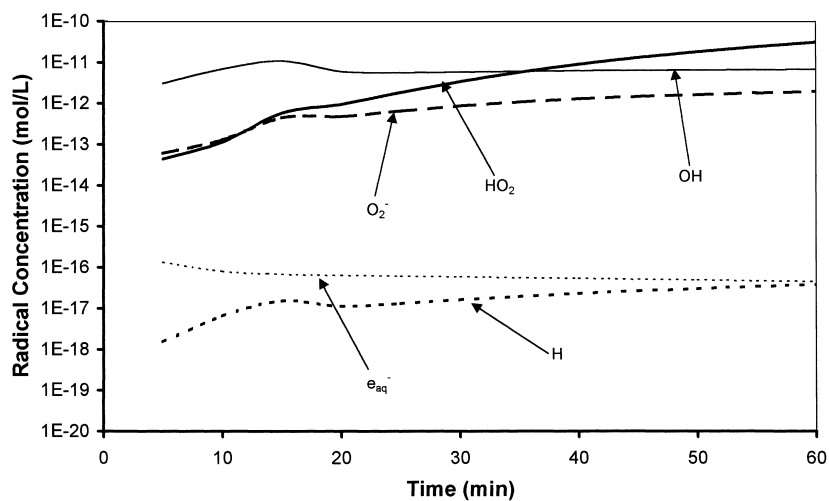


Fig. 15. Kinetic simulations showing radical concentrations for 57 kV pulsed corona treatment and $485 \mu\text{M}$ FeSO_4 (initial phenol concentration = 0 ppm).

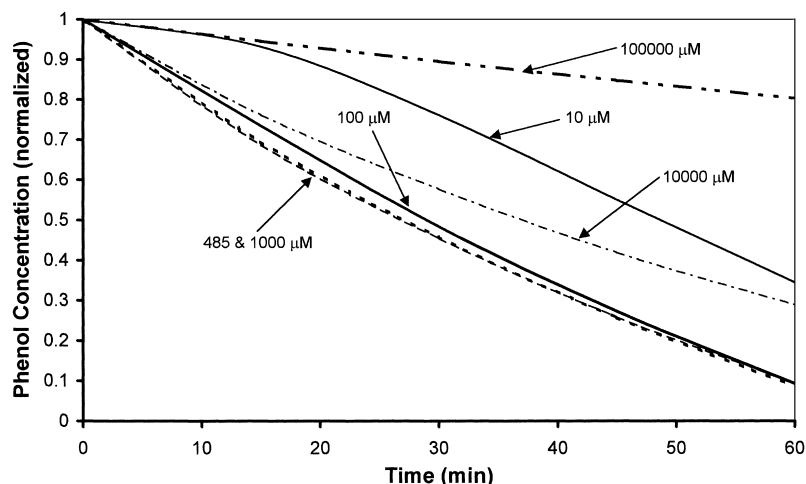


Fig. 16. Kinetic simulations showing the effect of iron concentration on phenol degradation for 57 kV pulsed corona treatment (initial phenol concentration = 100 ppm).

Fig. 4 there are large differences in the amounts of phenol removed from the solution in 60 min. As the iron concentration increases, the solution conductivity increases, thus decreasing the rate of hydrogen peroxide formation in solution as shown in Fig. 4. This leads to the decrease in the amount of phenol removed with increasing ferrous sulfate shown in the model simulation in Fig. 17.

To determine the extent of radical formation by direct reactions from the corona discharge relative to radical formation from indirect reactions of hydrogen peroxide, the model was run neglecting reactions (1) and (3) and only considering the corona-induced reaction (2). All radical species would therefore only be formed by indirect reaction from hydrogen peroxide. This simulation (not shown here) showed radical

concentrations nearly identical to those in the case where the hydroxyl radical, hydrogen radical, and aqueous electron are produced directly by the corona discharge (i.e. including reactions (1)–(3)). This shows that the rates of formation of the radicals are more sensitive to the chemical reactions occurring indirectly from hydrogen peroxide than to the rate of production directly from the pulsed corona discharge.

Furthermore, one of the major assumptions used in the model development was the hypothesis that all species produced by the pulsed corona discharge were formed homogeneously throughout the reactor volume. It is likely that for pulsed electrical discharges in water, the radical species, including hydroxyl radical, hydrogen radical, and aqueous electrons, are produced either within the discharge

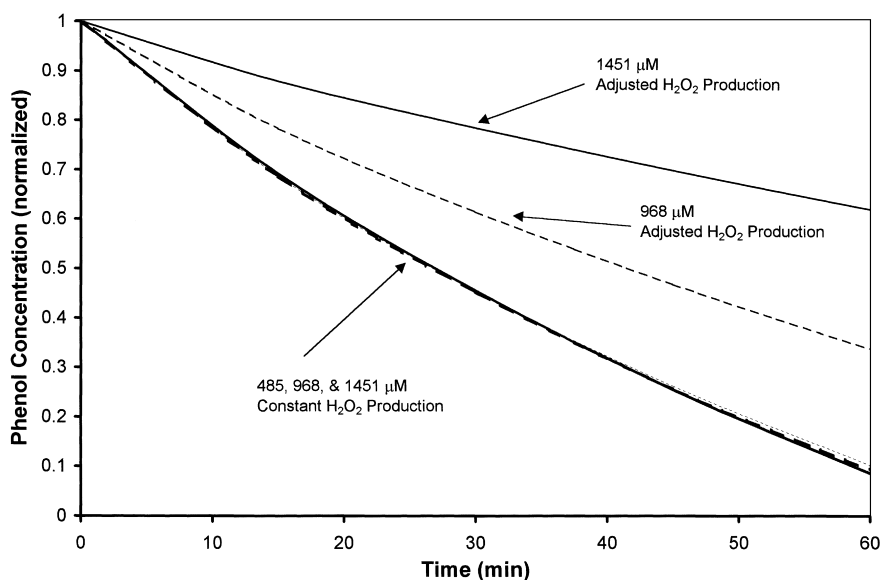


Fig. 17. Kinetic simulations showing the effect of iron concentration and hydrogen peroxide formation rates on phenol degradation for 57 kV pulsed corona treatment (initial phenol concentration = 100 ppm).

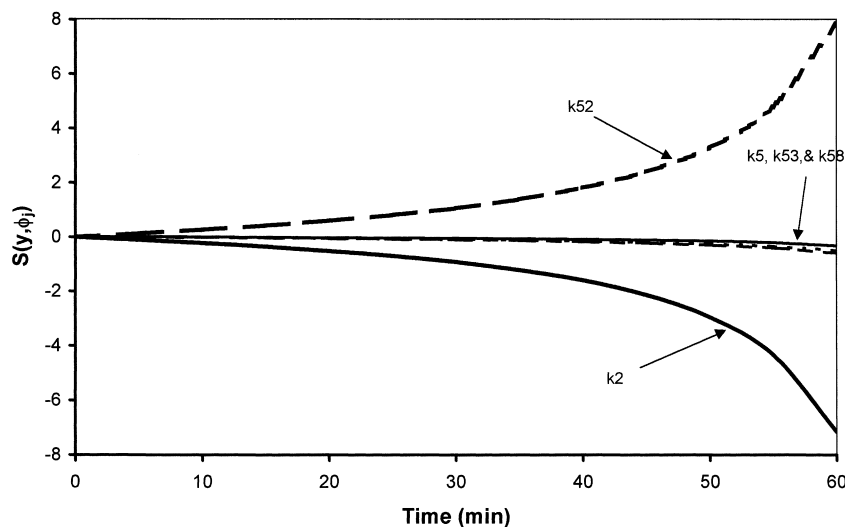


Fig. 18. The dimensionless sensitivity coefficients for phenol concentration with respect to reaction rate constants for the five most important chemical reactions as a function of time.

(streamer) or intimately close to the discharge region in a non-homogeneous manner. The fact that the model results are insensitive to direct corona-induced radical formation supports the hypothesis that the major species formed locally in the streamer is hydrogen peroxide and that the hydrogen peroxide diffuses into the bulk from the streamers. This result also supports the hypothesis that the other radical species formed in the streamer react and recombine in these local regions.

Results from the sensitivity analysis are given in Figs. 18 and 19. Fig. 18 shows the non-dimensional sensitivity coefficients for the phenol concentration with respect to the five most important reactions over a 60 min time interval. These

reactions had the highest absolute value of the normalized sensitivity coefficients at 60 min. Fig. 19 shows values of the normalized sensitivity coefficients at 60 min for the 10 most important reactions.

The sensitivity analysis shows that the most important reaction in the present system is the dissociation of hydrogen peroxide by reaction (52), followed closely by the production of hydrogen peroxide by the corona discharge (reaction (2)). As shown in Fig. 18, the normalized sensitivity coefficients for the dissociation of the hydrogen peroxide by reaction (52) increases with time, which indicates that increases in this reaction rate constant causes the concentration of phenol in the system to increase. Since

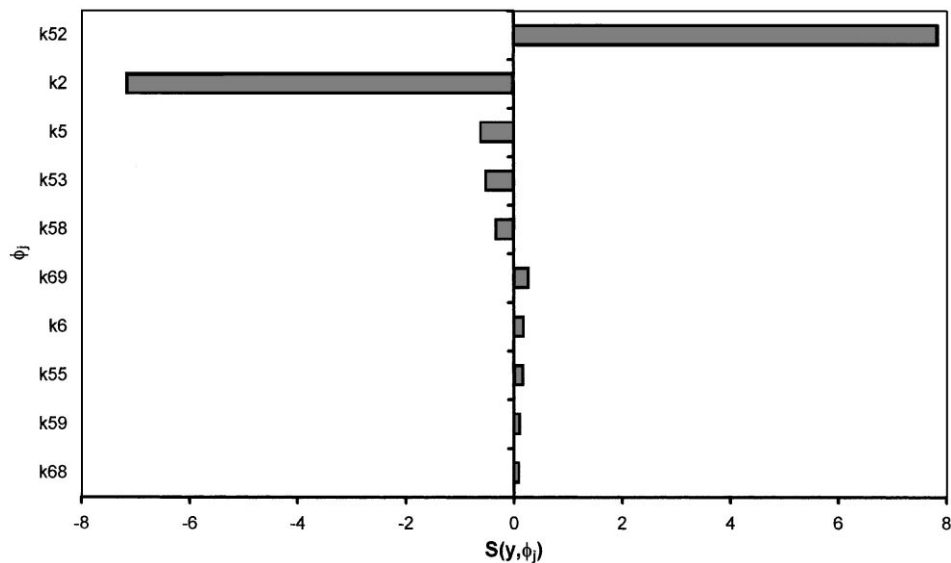


Fig. 19. The peak values of the dimensionless sensitivity coefficients for phenol concentration with respect to reaction rate constants for the 10 most important chemical reactions.

reaction (52) represents a loss of hydrogen peroxide without the formation of active hydroxyl radicals, an increase in the rate of this reaction would reduce phenol removal, i.e. increase phenol concentration, because less hydroxyl radicals would be available for reaction with the phenol. Similarly, if the rate of production of hydrogen peroxide increased in reaction (2), the concentration of phenol would decrease, thus giving negative sensitivity coefficients. The third most important reaction is the Fenton's reaction (reaction (5)), which would cause the concentration of phenol to decrease as the reaction rate constant for the Fenton's reaction increases.

5. Conclusions

The present study demonstrates, using experimental data and computer simulations, the important role of Fenton's reaction chemistry on the degradation of organic compounds, specifically phenol, in liquid phase pulsed corona reactors. The rate of hydrogen peroxide formation in the pulsed corona reactor is dependent upon both the solution conductivity and the applied electrical potential. For both applied voltages considered the rate of formation of hydrogen peroxide decreased monotonically with increasing solution conductivity. A mathematical model, including 31 species and 71 reactions, was developed using known chemical reactions and reaction rate constants from the radiation chemistry literature and the literature on Fenton's chemistry. Experimental measurements in the pulsed corona reactor of the rate of hydrogen peroxide formation in the absence of organic compounds and iron salts are incorporated within the model. The resulting model, containing no fitting parameters, describes the effects of initial iron and phenol concentrations on the degradation of phenol and the formation of by-products. This result indicates that under the given conditions of approximately 1 J per pulse discharge, the bulk phase chemical reactions in the pulsed corona reactor can be described fairly well by known chemical reactions. It is important to note that at conductivity near and above the limits used in the present study, other factors, including possible iron flocculation and the production of ultraviolet light may become important.

Acknowledgements

We would like to acknowledge partial support from the Department of Chemical Engineering, FAMU-FSU College of Engineering, and some equipment supplied by the Electronics Division of the US Air Force, Tyndall AFB. We are indebted to Dr. Joseph Pignatello for assistance with the Fenton's chemistry and for providing us helpful information on the analysis of Fenton's reactions. We would also like to thank Mr. Mike Kirkpatrick, Mr. Jason Maxwell, and Mr. Giridhar Sathiamoorthy for assistance in the laboratory

and Dr. Ronald J. Clark for discussions on chemical analysis methods.

References

- [1] T.J. Gallagher, *Simple Dielectric Liquids: Mobility, Conduction, Breakdown*, Clarendon Press, Oxford, 1975.
- [2] H.M. Jones, E.E. Kunhardt, *J. Appl. Phys.* 77 (1995) 795.
- [3] H.M. Jones, E.E. Kunhardt, *J. Phys. D: Appl. Phys.* 28 (1995) 178.
- [4] A.J.H. Sale, W.A. Hamilton, *Biochim. Biophys. Acta* 148 (1967) 781.
- [5] W.A. Hamilton, A.J.H. Sale, *Biochim. Biophys. Acta* 148 (1967) 789.
- [6] J.C. Weaver, Y.A. Chizmadzhev, *Bioelectrochem. Bioenergetics* 41 (1996) 135.
- [7] M. Sato, T. Ohgiyama, J.S. Clements, *IEEE Trans. Ind. Appl.* 32 (1996) 106.
- [8] A.K. Sharma, B.R. Locke, P. Arce, W.C. Finney, *Hazard. Waste Hazard. Mater.* 10 (1993) 209.
- [9] P. Sunka, V. Babicky, M. Clupek, P. Lukes, M. Simek, J. Schmidt, M. Cernak, *Plasma Sources Sci. Technol.* 8 (1999) 258.
- [10] B. Sun, M. Sato, J.S. Clements, *Environ. Sci. Technol.* 34 (2000) 509.
- [11] M. Sato, T. Ohgiyama, S. Clements, *IEEE Trans. Ind. Appl.* 32 (1996) 106.
- [12] A. Mizuno, Y. Hori, *IEEE Trans. Ind. Appl.* 24 (1988) 387.
- [13] A. Mizuno, T. Inoue, S. Yamaguchi, K. Sakamoto, T. Saeki, Y. Matsumoto, K. Minamiyama, *Inactivation of viruses using pulsed high electric fields*, Conference Record of the IEEE-IAS, 1990, pp. 77–83.
- [14] M. Sato, K. Tokita, M. Sadakata, T. Sakai, K. Nakanishi, *Int. Chem. Eng.* 30 (1990) 695.
- [15] T. Grahl, H. Maerkl, *Appl. Microbiol. Biotech.* 45 (1996) 148.
- [16] B.R. Locke, P. Sunka, M. Sato, J.S. Chang, *Non-thermal plasma and electrohydraulic discharge water treatment*, in: H. Al-Ekabi (Ed.), *Advanced Oxidation Technologies, Fundamentals and Environmental Applications*, Wiley, New York, 2001, in press.
- [17] M.R. Hoffmann, I. Hua, R. Hochemer, D. Willberg, P. Lang, A. Kratel, *Chemistry under extreme conditions in water induced electrohydraulic cavitation and pulsed-plasma discharges*, in: R. van Eldik, C.D. Hubbard (Eds.), *Chemistry Under Extreme or Non-Classical Conditions*, Wiley, New York, 1997.
- [18] S.M. Korobeinikov, E.V. Yanshin, *Sov. Phys. Tech. Phys.* 28 (1983) 1288.
- [19] J.W. Robinson, M. Ham, A.N. Balaster, *J. Appl. Phys.* 44 (1973) 72.
- [20] J.W. Robinson, *J. Appl. Phys.* 38 (1967) 210.
- [21] H.M. Jones, E.E. Kunhardt, *IEEE Trans. Dielectrics Electr. Insul.* 1 (1994) 1016.
- [22] J.S. Clements, M. Sato, R.H. Davis, *IEEE Trans. Ind. Appl.* IA-23 (1987) 224.
- [23] C. Walling, *Accounts Chem. Res.* 8 (1975) 125.
- [24] C. Walling, T. Weil, *Int. J. Chem. Kin.* 6 (1974) 507.
- [25] A.K. Sharma, *High voltage pulsed streamer corona discharges for the removal of organic contaminants from aqueous solutions*, masters of science, FAMU-FSU College of Engineering, Florida Agricultural and Mechanical University, Tallahassee, FL, 1993.
- [26] A.A. Joshi, B.R. Locke, P. Arce, W.C. Finney, *J. Hazard. Mater.* 41 (1995) 3.
- [27] N.I. Kuskova, *Sov. Phys. Tech. Phys.* 28 (1983) 591.
- [28] G.V. Buxton, *Radiation chemistry of the liquid state. 1. Water and homogeneous aqueous solutions*, in: Farhataziz, M.A.J. Rodgers (Eds.), *Radiation Chemistry, Principles and Applications*, VCH, Weinheim, Germany, 1987.
- [29] B. Sun, M. Sato, A. Harano, J.S. Clements, *J. Electrostatics* 43 (1998) 115.

- [30] B. Sun, M. Sato, J.S. Clements, *J. Electrostatics* 39 (1997) 189.
- [31] Y. Sun, J.J. Pignatello, *J. Agric. Food Chem.* 40 (1992) 322.
- [32] Y. Sun, J.J. Pignatello, *J. Agric. Food Chem.* 41 (1993) 308.
- [33] J.J. Pignatello, K. Baehr, *J. Environ. Quality* 23 (1994) 365.
- [34] J.J. Pignatello, M. Day, *Hazard. Waste Hazard. Mater.* 13 (1996) 237.
- [35] Y. Sun, J.J. Pignatello, *Environ. Sci. Technol.* 27 (1993) 304.
- [36] J.J. Pignatello, *Environ. Sci. Technol.* 26 (1992) 944.
- [37] W.G. Kuo, *Water Res.* 26 (1992) 881.
- [38] F.J. Potter, J.A. Roth, *Hazard. Waste Hazard. Mater.* 10 (1993) 151.
- [39] A.P. Murphy, W.J. Boegli, M.K. Price, C.D. Moody, *Environ. Sci. Technol.* 23 (1989) 166.
- [40] R. Venkatadri, R.W. Peters, *Hazard. Waste Hazard. Mater.* 10 (1993) 107.
- [41] J.M. Joseph, H. Destaillets, H.M. Hung, M.R. Hoffmann, *J. Phys. Chem.* 104 (2000) 301.
- [42] B. Srinivasan, S. Palanki, D. Grymonpre, B.R. Locke, *Chem. Eng. Sci.*, 2001, in press.
- [43] D. Grymonpre, W.C. Finney, B.R. Locke, *Chem. Eng. Sci.* 54 (1999) 3095.
- [44] E.J. Hart, *J. Am. Chem. Soc.* 73 (1951) 68.
- [45] C.J. Hohanadel, *J. Phys. Chem.* 56 (1952) 587.
- [46] R. Chen, J.J. Pignatello, *Environ. Sci. Technol.* 31 (1997) 2399.
- [47] C. Walling, A.J. Goosen, *J. Am. Chem. Soc.* 95 (1973) 2987.
- [48] J.D. Rush, B.H.J. Bielski, *J. Phys. Chem.* 89 (1985) 5062.
- [49] C.D. Jonah, J.R. Miller, M.S. Matheson, *J. Phys. Chem.* 81 (1977) 1618.
- [50] J.H. Baxendale, R.S. Dixon, D.A. Stott, *Trans. Faraday Soc.* 64 (1968) 2398.
- [51] B.H.K. Bielski, D.E. Cabelli, R.L. Arudi, A.B. Ross, *J. Phys. Chem. Ref. Data* 14 (1985) 1041.
- [52] H. Christensen, K. Sehested, *J. Phys. Chem.* 87 (1983) 118.
- [53] A.J. Elliot, G.V. Buxton, *J. Chem. Soc., Faraday Trans.* 88 (1992) 2465.
- [54] D. Zehavi, J. Rabani, *J. Phys. Chem.* 75 (1971) 1738.
- [55] J. Rabani, M.S. Matheson, *J. Phys. Chem.* 70 (1966) 761.
- [56] H. Christensen, K. Sehested, H. Corfitzen, *J. Phys. Chem.* 86 (1982) 1588.
- [57] H.A. Schwarz, *J. Phys. Chem.* 96 (1992) 8937.
- [58] A.J. Elliot, D.R. McCracken, G.V. Buxton, N.D. Wood, *J. Chem. Soc., Faraday Trans.* 86 (1990) 1539.
- [59] W. Gruenbein, A. Henglein, G. Stevens, G. Beck, *Ber. Bunsenges. Phys. Chem.* 75 (1971) 126.
- [60] W.D. Felix, B. Gall, L.M. Dorfman, *J. Phys. Chem.* 71 (1967) 384.
- [61] M.S. Matheson, J. Rabani, *J. Phys. Chem.* 69 (1965) 1324.
- [62] P.Y. Feng, A. Brynjolfsson, J.W. Halliday, R.D. Jarrett, *J. Phys. Chem.* 74 (1970) 1221.
- [63] J.K. Thomas, *Trans. Faraday Soc.* 61 (1965) 702.
- [64] A.J. Elliot, *Rad. Phys. Chem.* 34 (1989) 753.
- [65] B. Hickel, K. Sehested, *J. Phys. Chem.* 95 (1991) 744.
- [66] N.V. Raghavan, S. Steenken, *J. Am. Chem. Soc.* 102 (1980) 3495.
- [67] P. O'Neill, S. Steenken, D. Schulte-Frohlinde, *J. Phys. Chem.* 79 (1975) 2773.
- [68] K.B. Patel, R.L. Willson, *J. Chem. Soc., Faraday Trans.* 69 (1973) 814.
- [69] J.H. Baxendale, H.H. Hardy, L.H. Sutcliffe, *Trans. Faraday Soc.* 47 (1951) 963.
- [70] E. Mentasti, E. Pelizzetti, G.J. Saini, *J. Chem. Soc., Dalton Trans.* 19 (1973) 2609.
- [71] T.D. Thornton, D. LaDue, P.E. Savage, *Environ. Sci. Technol.* 25 (1991) 1507.
- [72] T.D. Thornton, P.E. Savage, *AIChE J.* 38 (1992) 321.
- [73] M. Krajnc, J. Levec, *AIChE J.* 42 (1996) 1977.
- [74] C. Petrier, M. Micolle, G. Merlin, J.L. Lucche, G. Reverdy, *Environ. Sci. Technol.* 26 (1992) 1639.
- [75] S.J. Neigowski, *Ind. Eng. Chem.* 45 (1953) 632.
- [76] H.R. Eisenhauer, *J. Water Poll. Con. Fed.* 40 (1968) 1887.
- [77] H.S. Joglekar, S.D. Samant, J.B. Joshi, *Water Res.* 25 (1991) 135.
- [78] W.F.L.M. Hoeben, Pulsed corona-induced degradation of organic materials in water, Ph.D. Thesis, Technische Universiteit Eindhoven, 2000.
- [79] A. Varma, M. Morbidelli, H. Wu, *Parametric Sensitivity in Chemical Systems*, Cambridge University Press, Cambridge, 1999.
- [80] P. Lukes, P. Sunka, M. Clupek, V. Babicky, V. Janda, J. Novak, J.D. Skalny, Role of various parameters on production of H₂O₂ by pulsed corona discharge in water, in: *Proceedings of the 6th International Conference on Advanced Oxidation Technologies for Water and Air Remediation*, London, Ont., Canada, 26–30 June 2000.